

The Plant Cell, Vol. 22: 3804–3815, November 2010, www.plantcell.org © 2010 American Society of Plant Biologists

***Arabidopsis* Kinetochore Fiber-Associated MAP65-4 Cross-Links Microtubules and Promotes Microtubule Bundle Elongation**

Vincent Fache,^a Jérémie Gaillard,^a Daniel Van Damme,^{b,c} Danny Geelen,^d Emmanuelle Neumann,^e Virginie Stoppin-Mellet,^a and Marylin Vantard^{a,1}

^a Institut de Recherches en Technologies et Sciences pour le Vivant, Commissariat à l’Energie Atomique/Centre National de la Recherche Scientifique/Institut National de la Recherche Agronomique/Université Joseph Fourier, 38054 Grenoble, France

^b Department of Plant Systems Biology, VIB, B-9052 Ghent, Belgium

^c Department of Plant Biotechnology and Genetics, Ghent University, B-9052 Ghent, Belgium

^d Department of Plant Production, Ghent University, B-9000 Ghent, Belgium

^e Institut de Biologie Structurale, Commissariat à l’Energie Atomique/Centre National de la Recherche Scientifique/Université Joseph Fourier, 38027 Grenoble, France

The acentrosomal plant mitotic spindle is uniquely structured in that it lacks opposing centrosomes at its poles and is equipped with a connective preprophase band that regulates the spatial framework for spindle orientation and mobility. These features are supported by specialized microtubule-associated proteins and motors. Here, we show that *Arabidopsis thaliana* MAP65-4, a non-motor microtubule associated protein (MAP) that belongs to the evolutionarily conserved MAP65 family, specifically associates with the forming mitotic spindle during prophase and with the kinetochore fibers from prometaphase to the end of anaphase. In vitro, MAP65-4 induces microtubule (MT) bundling through the formation of cross-bridges between adjacent MTs both in polar and antipolar orientations. The association of MAP65-4 with an MT bundle is concomitant with its elongation. Furthermore, MAP65-4 modulates the MT dynamic instability parameters of individual MTs within a bundle, mainly by decreasing the frequency of catastrophes and increasing the frequency of rescue events, and thereby supports the progressive lengthening of MT bundles over time. These properties are in line with its role of initiating kinetochore fibers during prospindle formation.

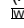
INTRODUCTION

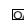
In plant cells, microtubule (MT) cytoskeleton arrays provide a molecular framework for various cellular processes, including cell morphogenesis, establishment of cell polarity, and cell division (Ehrhardt, 2008). Higher plant MT arrays do not emanate as radial arrays from a well-defined MT-organizing center (i.e., the centrosome). Instead, they are composed mainly of MT bundles, which are highly dispersed within the cell cortex during interphase (and known as cortical MTs) or organized as a mitotic spindle during cell division. In addition, plant cells organize a ring of MT bundles at the onset of mitosis, called the preprophase band (PPB). This PPB defines the future division plane and the position of interdigitated MT bundles at the midzone during cytokinesis, a structure referred to as the phragmoplast. The bundling of MTs is a crucial step in the formation and stabilization of MT arrays throughout the cell cycle and hinges on the ability of

the cytoskeleton to auto-organize into higher-order structures. Although the basic MT behavior necessary for creating and organizing cortical MT bundles has been revealed by dynamic imaging and genetic studies (Ehrhardt, 2008; Wasteneys and Ambrose, 2009), our knowledge of the organization and functioning of MT bundles within the acentrosomal plant mitotic spindle is limited (Bratman and Chang, 2007). The cortical array is a self-organizing cortical network that arranges its MTs via a sequence of events: MT nucleation at dispersed sites within the lattice of preexisting MTs (Murata et al., 2005; Chan et al., 2009), release of MTs from their nucleation sites (Shaw et al., 2003; Stoppin-Mellet et al., 2006), and transport of the MTs by a hybrid treadmilling mechanism (Shaw et al., 2003). The angle at which MTs encounter other MTs determines the outcome of the MT interaction; it can cause catastrophe, severing, crossover, or bundling (Shaw et al., 2003; Dixit and Cyr, 2004). The cumulative effect of these outcomes underpins the self-ordering characteristics of the MT networks and forms the basis of the properties of the different arrays (Wasteneys and Ambrose, 2009). MT bundling is particularly important during mitosis because it facilitates polarity establishment of the acentrosomal bipolar spindle by selectively stabilizing polar and antipolar MTs. Several types of proteins and cellular structures play a role in grouping or bundling MTs together. The kinetochores are the docking sites for the MT plus ends, bridging MTs together that make up a kinetochore

¹ Address correspondence to marylin.vantard@cea.fr.

The author responsible for distribution of materials integral to the findings presented in this article in accordance with the policy described in the Instructions for Authors (www.plantcell.org) is: Marylin Vantard (marylin.vantard@cea.fr).

 Online version contains Web-only data.

 Open Access articles can be viewed online without a subscription. www.plantcell.org/cgi/doi/10.1105/tpc.110.080606

fiber (McDonald et al., 1992). At the minus end, plants do not attach the kinetochore MTs to a spindle pole body or a centrosome. Instead, pole focusing of the kinetochore fibers has been proposed to rely on minus end-directed motors that may form cross-links between individual MTs (Smirnova et al., 1998; Chen, 2002; Ambrose et al., 2005). Selective cross-linking of non-kinetochore MTs takes place at the spindle midzone and maintains spindle bipolarity. *Arabidopsis* kinesin-14 (ATK5), which belongs to the kinesin-14 family, is thought to mediate lateral interactions to coalign MTs into linear bundles in regions of overlap between interpolar MTs (Ambrose and Cyr, 2007). Another group of proteins that bundle MTs in vitro, namely, the MAP65 family in plants, and its homologs, Ase1 in fungus (Janson et al., 2007) and PRC1 in mammals (Mollinari et al., 2002), have been implicated in these interactions. In the plant model *Arabidopsis thaliana*, nine members of this family were identified that share between 28 and 79% amino acid identity (Hussey et al., 2002). To date, only *Arabidopsis* MAP65-1, MAP65-5, and MAP65-2 have been shown to induce MT bundling in vitro (Chan et al., 1999; Smertenko et al., 2004; Gaillard et al., 2008; Li et al., 2009). Electron microscopy of MAP65-1 and MAP65-5 in in vitro preparations showed the formation of filamentous cross-bridges at regular intervals along MT walls with an angle of 60° between antipolar MTs (Gaillard et al., 2008). In vivo, MAP65-1 and MAP65-5 MT bundles are associated with the cellular cortex and the interzonal region during anaphase (Chan et al., 1999; Smertenko et al., 2004; Gaillard et al., 2008). MAP65-2 induces stable MT bundles in vitro and is localized with almost all of the MT arrays present in plant cells (Li et al., 2009). The biochemical properties of the remaining MAP65s are not known, and most studies have focused on their subcellular localization using antibodies and green fluorescent protein (GFP) tagging. MAP65-3 is associated with the mitotic spindle during both early and late mitosis in all *Arabidopsis* organs (Müller et al., 2004; Caillaud et al., 2008). MAP65-4 localization has been associated with the metaphase and anaphase spindle MTs when fused to GFP in tobacco (*Nicotiana tabacum*) BY-2 cells (Van Damme et al., 2004), whereas it has been described to localize at the midzone of the spindle during anaphase and with phragmoplast MTs using immunostaining methods (Smertenko et al., 2008). Immunostaining methods have localized MAP65-6 to mitochondria (Mao et al., 2005) or to the anaphase spindle (Smertenko et al., 2008). On the basis of these different studies, it appears that, for at least some members of the *Arabidopsis* MAP65 family, their localization within cells is rather complex. Further biochemical characterization of MAP65 proteins will be required to establish what function individual members play in the organization of the acentrosomal MT cytoskeleton.

Here, we report on the biochemical and functional properties of MAP65-4. In vitro, MAP65-4-bundled MTs maintained an intermicrotubule spacing of ~15 nm, and the angle between MAP65-4 and the MT lattice was 90°. Further analysis of the dynamic behavior of individual MTs within MAP65-4 bundles revealed that it regulates dynamic instability of MTs mostly by decreasing catastrophe and increasing rescue events. Interestingly, the duration of depolymerization phases was shortened and that of elongation phases was increased, supporting the progressive lengthening of MT bundles over time. In vivo,

MAP65-4 is strictly localized with MTs during mitosis, specifically with MTs of the forming mitotic spindle during prophase and with the kinetochore fibers from prometaphase to the end of anaphase. Thus, our observations argue that MAP65-4 mediates lateral interactions between spindle MTs, where it may participate in the formation and dynamics of MTs within kinetochore fibers.

RESULTS

MAP65-4 Is Localized to Kinetochore Fibers during Mitosis

To identify the MT array with which MAP65-4 is associated, the cellular distribution of GFP-tagged recombinant protein was investigated in tobacco BY-2 cells (Figure 1; see Supplemental Movies 1 and 2 online). In the more than 100 independent transgenic lines analyzed, GFP-AtMAP65-4 expression was detected in mitotic cells (see Supplemental Figure 1A and Supplemental Movies 1 and 2 online). The majority of interphase cells did not fluoresce, and ~10% of the lines showed weak fluorescence in the nucleus (Figure 1B). In contrast with the MT binding preference of other members of the MAP65 family analyzed to date (Caillaud et al., 2008; Gaillard et al., 2008; Li et al., 2009), MAP65-4 was not associated with MTs of the PPB (Figure 1A). MAP65-4 localized exclusively to the perinuclear MTs in early prophase cells (Figure 1B). Upon bipolarization of the perinuclear MT array, MAP65-4 started to accumulate at the two sides of the nucleus that corresponded to the future poles of the spindle (Figure 1B; see Supplemental Figure 1B and Supplemental Movies 1 and 2 online). Later on, during nuclear envelope breakdown (NEB), GFP-MAP65-4 was associated with MTs that invaded the nuclear space (Figure 1C; see Supplemental Movies 1 and 2 online). In fully matured spindles, GFP-MAP65-4 was associated with the kinetochore fibers (Figure 1E). During cytokinesis, in some cells, weak GFP-AtMAP65-4 signal was observed at the level of the cell plate (Figure 1B). Quantification of the GFP fluorescence signal intensity showed that the levels increased from preprophase to anaphase and then rapidly decreased, suggesting proteolytic removal of GFP-MAP65-4 at the end of anaphase to early telophase (see Supplemental Figure 1 online).

AtMAP65-4 Induces MT Bundling in Vitro

To investigate the biochemical properties of MAP65-4 in vitro, recombinant His-MAP65-4-His and GFP-MAP65-4-His proteins were purified as previously described (Gaillard et al., 2008). Incubation of His⁶MAP65-4-His (from 0.1 to 0.5 μM) with taxotere-stabilized Alexa488-labeled MTs (0.5 μM) stimulated the formation of MT bundles (Figure 2A, a to c). GFP-MAP65-4-His was equally active than on MAP65-4 fused to GFP in bundling MTs and homogeneously stained MT bundles (see Supplemental Figure 2 online). Single MT strands did not accumulate MAP65-4, suggesting that bundling of the MTs stabilized the MT-MAP65-4 interactions. Analyses of electron micrographs of MAP65-4-induced bundles showed that MTs were parallel to each other and separated by 15-nm cross-bridges (Figure 2B, a to c). The cross-bridges formed a lattice that was equally spaced along MT

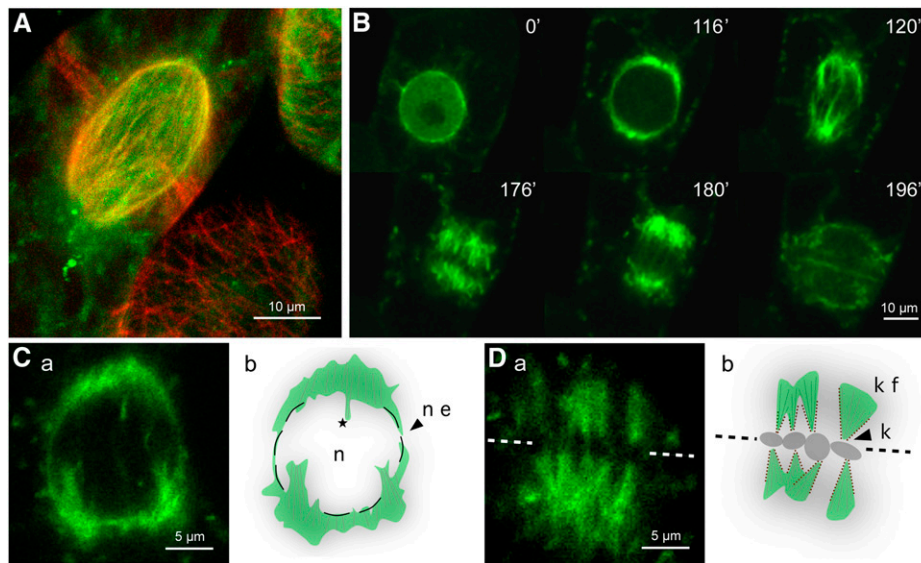


Figure 1. MAP65-4 Localizes to the Forming Mitotic Spindle and Kinetochore Fibers

(A) Dual labeling of tobacco BY-2 cells expressing MAP65-4-GFP and RFP-TUA6. During prophase, MAP65-4-GFP strongly bound perinuclear MTs (top left cell). In interphase cells, MAP65-4 did not associate with the cortical MT network (bottom right cell).

(B) Time-lapse recording of tobacco BY-2 cells expressing MAP65-4-GFP during cell division. From G2 ($t = 0$) to prophase ($t = 116'$), MAP65-4-GFP accumulated at the perinuclear MT basket. At the prophase/prometaphase transition, the MTs reorganized and formed two poles from which MT bundles emanated toward the liberated chromosomes ($t = 120'$). AtMAP65-4 labeled the kinetochore MTs as the spindle formed, from prometaphase ($t = 176'$) to late anaphase ($t = 180'$).

(C) and **(D)** MAP65-4-GFP localization during nuclear envelope breakdown **(C)** and metaphase **(D)**. **(Cb)** and **(Db)** are cartoon representations of **(Ca)** and **(Da)**, respectively. n, nucleus; ne, nuclear envelope; star, MTs that invade the nuclear space; k, kinetochore; kf, kinetochore fiber. The equatorial plane is defined by the dotted line and chromosomes are represented by gray circles.

walls, at a distance of 15 to 17 nm for a 1:1 stoichiometric ratio of tubulin dimers and MAP65-4. This distance corresponds to the binding of one MAP65-4 protein every second tubulin dimer. The angle between the cross-bridges relative to the MT axis was 90° .

In a complementary series of experiments, we performed a truncation analysis of MAP65-4 to identify domains responsible for MT binding and bundling. Three different domains corresponding to the N-terminal, the central, and the C-terminal regions of MAP65-4 (referred to as domains 1, 2, and 3, respectively) were defined on the basis of the amino acid sequence alignment of MAP65s (Figure 3). In addition, domain 3 (the C-terminal region) was subdivided in two domains: the N-terminal part, which includes the most evolutionarily conserved domain of the MAP65 family (referred to as 3N), and the C-terminal part, which is divergent among the MAP65 members (referred to as 3C) (Figure 3A). High-speed centrifugation of MAP65-4 and of truncated proteins after incubation with MTs demonstrated that MT binding activity is localized to 3N (see Supplemental Figure 3 online). Hence, the MT binding domain of MAP65-4 is located in the evolutionarily conserved part of MAP65s, in agreement with the position of the MT binding domain in MAP65-1 and MAP65-5 (Gaillard et al., 2008). In addition, the efficiency of MT bundling by the different full-length and truncated MAP65-4 proteins was assayed by low-speed centrifugations that allowed single MTs to remain in the supernatant, while bundled MTs were sedimented (Figure 3B), and by fluorescence microscopy imaging assays

(Figure 3C). These experiments revealed that the N-terminal, the central, and the 3N domains independently contributed to the MT bundling activity, whereas the 3C domain did not (Figure 3).

To discriminate between the amino acid sequences involved in MT bundling and MT binding in the 3N domain, we produced three different peptides with deletions in the N- or C-terminal part of this domain (sequences 338 to 452 amino acids, 320 to 452 amino acids, and 338 to 476 amino acids), and MAP65-4 deleted of the sequence amino acids 440 to 472 [MAP65-4 ($\Delta 440-472$)] (see Supplemental Figure 3 online). None of these constructs were able to bind to MTs. Thus, the 3N domain as defined in this study is strictly necessary for the binding of MAP65-4 to MTs and is involved in MT bundling activities.

MAP65-4 Affects MT Dynamics within Bundles

To elucidate the molecular mechanisms by which MAP65-4 generates MT bundles and influences their dynamics, we developed a real-time *in vitro* assay in which the dynamic instability behavior of individual MTs within bundles could be determined. This was done by implementing a dual-color total internal reflection fluorescence (TIRF) assay in reconstitution experiments (described in Methods). Alexa568-labeled tubulin was polymerized in the presence of GMPCPP to obtain stable MT seeds that were incubated with $0.1 \mu\text{M}$ MAP65-4. Short bundles were produced, referred to as MT seed bundles, which were

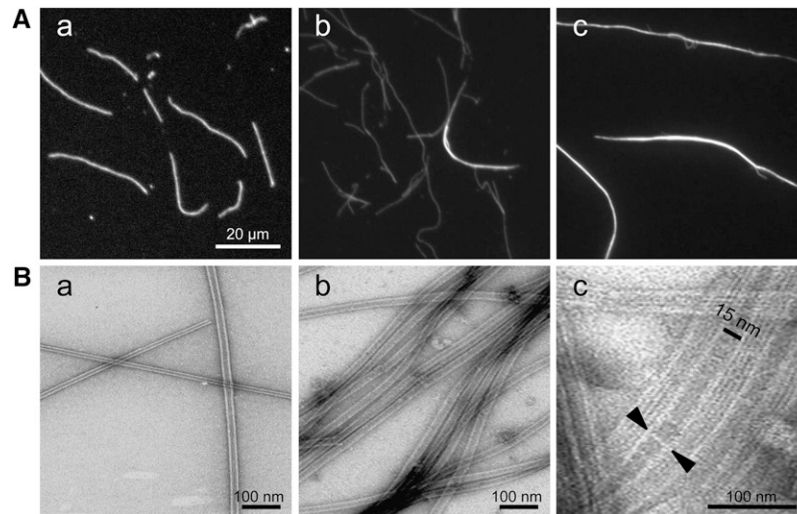


Figure 2. MAP65-4 Induces MT Bundling through the Formation of 15-nm Cross-Bridges in Vitro.

(A) Rhodamine-labeled taxotere-stabilized MTs ($0.5 \mu\text{M}$) incubated in the absence **(a)** or presence of $0.1 \mu\text{M}$ **(b)** and $0.5 \mu\text{M}$ **(c)** AtMAP65-4. **(B)** Negatively stained electron microscopy of MTs alone **(a)** or in the presence of MAP65-4 **(c)**. High-magnification view of MT bundles **(d)** shows MAP65-4 forming extensive inter-MT bridges of 15 nm (arrows). The bridges are oriented at an angle of $\sim 90^\circ$ relative to the lattice of MTs.

elongated by the addition of Alexa488-labeled tubulin and various concentrations of MAP65-4 (Figure 4A). As controls, single MT seeds were elongated by Alexa488-labeled tubulin in the absence of MAP65-4. This allowed us to determine the dynamic parameters of both MT ends of single MTs (Figure 4B, 1). At a given tubulin concentration, growth occurred mainly from the plus end, as expected, and could readily be visualized in kymographs (Figure 4B; see Supplemental Movie 3 online). The life history of the dynamic MT parameters at both MT ends is represented by triangles (in green) and the seed itself by a red line. Two of the three sides of the triangle represent an increase and decrease, respectively, in MT length over time. MTs within a bundle can be viewed as a superposition of several MT triangles (Figure 4B, 3).

The observation that MT bundle seed elongation occurs at similar rates at both ends suggests that MAP65-4-associated MTs have opposite polarity (Figure 4B, 2; see Supplemental Movie 4 online). To determine whether this polarity preference was an intrinsic property of MAP65-4, we analyzed mainly kymographs of MT bundles that have less than six MTs to allow the observation of MT minus ends; the MT ends of MT bundles that contain more MTs are embedded in the kymographs, rendering their detection difficult (Figure 4C, 2). The analysis showed that MT polarity within bundles was random, indicating that AtMAP65-4 bundled polar as well as antipolar MTs in vitro (Figure 4C).

We then examined if the presence of MAP65-4 would modify the dynamic parameters of bundled MTs. First, we measured the elongation and shortening speeds of the plus and minus ends of MTs assembled in the presence of various concentrations of MAP65-4 (Figure 5A). Single MTs showed a mean growth speed of $1.71 \pm 0.24 \mu\text{m}/\text{min}$ and a mean shrinkage speed of $16.55 \pm 4.99 \mu\text{m}/\text{min}$ at their MT plus end. The addition of $0.5 \mu\text{M}$

MAP65-4 did not change these parameters significantly (mean growth of $1.93 \pm 0.29 \mu\text{m}/\text{min}$ and mean shrinkage of $17.27 \pm 5.88 \mu\text{m}/\text{min}$). At the minus ends, single MTs showed a mean growth of $0.96 \pm 0.32 \mu\text{m}/\text{min}$ and a mean shrinkage speed of $17.3 \pm 3 \mu\text{m}/\text{min}$, and when bundled, they grew at a speed of $0.71 \pm 0.28 \mu\text{m}/\text{min}$ and shrank at a speed of $22.1 \pm 10.1 \mu\text{m}/\text{min}$. In conclusion, the elongation and shrinking rates were similar to values reported for single MTs and indicated that the bundling of MTs by MAP65-4 did not significantly affect their speed of elongation or shortening.

Next, we measured the frequency of catastrophe and rescue events of MTs when cross-linked by MAP65-4. These frequencies were defined as the ratio of catastrophe and rescue events during one measurement (recordings of ~ 25 min). For rescue events, we considered only situations of MT regrowth when the MTs did not depolymerize completely to the original seeds or seed bundles. Indeed, in our experimental set up, MT shrinkage down to MT seeds did not induce the complete disappearance of MTs, as the seeds were stabilized. Thus, MT regrowth from MT seeds could not be considered as a rescue event but rather as the assembly of a new MT. Increasing MAP65-4 concentrations from 0 to $0.5 \mu\text{M}$ led to a 36% ($n = 29$) reduction in catastrophe events at the MT plus ends and a 52.7% ($n = 29$) reduction at the MT minus ends within bundles (Figure 5B). In addition, the presence of $0.5 \mu\text{M}$ MAP65-4 led to an increase of 51% ($n = 29$) of rescue events at the MT plus ends and of 23.9% ($n = 29$) at their minus ends (Figure 5C). These measurements showed that, in the presence of MAP65-4, the frequency of catastrophe events for both MT ends decreased, whereas the frequency of rescue events at MT plus ends significantly increased. As a consequence, the duration of MT elongation in presence of $0.5 \mu\text{M}$ MAP65-4 increased on average from 3.5 min ($n = 173$) to 7.0 min ($n = 106$) for MT plus ends and from 5.0 min ($n = 109$) to 12.4 min

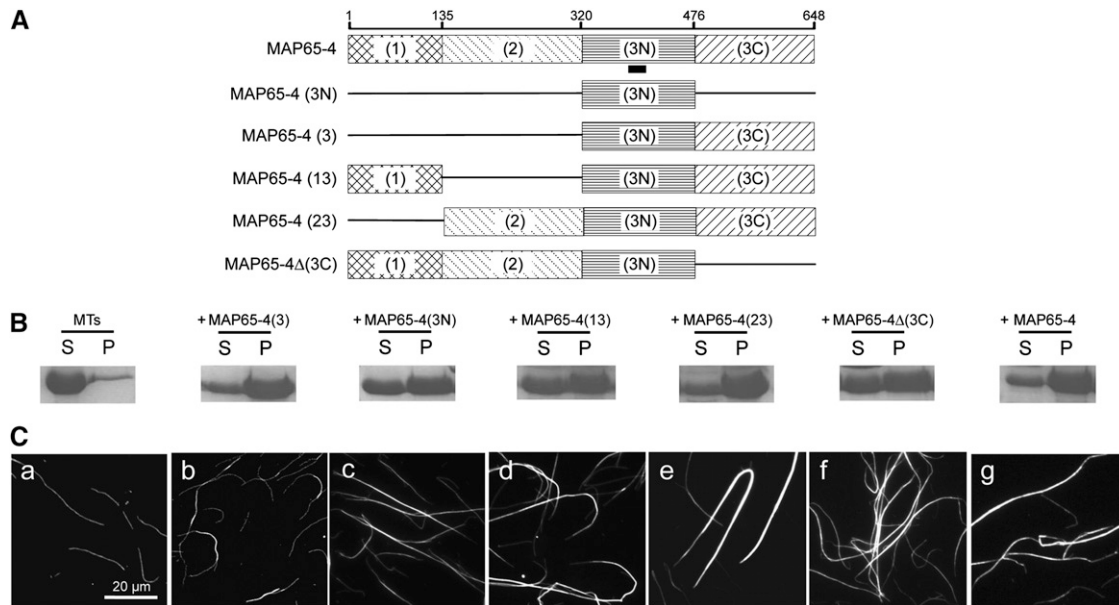


Figure 3. Identification of Functional Domains of MAP65-4 on MT Bundling Activity in Vitro.

(A) Diagrams of full-length MAP65-4 and its truncated domains. The conserved motif is underlined.

(B) Bundled MTs and individual MTs were separated by low-speed centrifugation, and pellets (P) and supernatants (S) were analyzed by SDS-PAGE. Full-length MAP65-4 and its different domains (1 μM) were incubated with 5 μM MTs.

(C) Rhodamine-labeled taxotere-stabilized MTs were incubated in the absence **(a)** or presence of MAP65-4(3) **(b)**, MAP65-4(3N) **(c)**, MAP65-4(13) **(d)**, MAP65-4(23) **(e)**, MAP65-4(Δ 3C) **(f)**, or MAP65-4 **(g)**. All of the proteins containing the 3N domain induced MT bundling.

($n = 48$) for MT minus ends (Figure 5D). These data are consistent with the observations showing that MT rescue events increased, whereas MT catastrophe events decreased in the presence of MAP65-4 (Figures 5A to 5C).

Finally, we examined the duration of the interval between catastrophe and rescue events. For that, we measured the length of MTs after a catastrophe event and calculated the ratio between the MT depolymerized lengths and the total distance between MT ends and the MT seed bundles (illustrated on kymographs, Figure 5E). The results are expressed as the distribution of the relative MT depolymerized lengths of all analyzed MTs (Figure 5F). In the absence of MAP65-4, the MT plus ends depolymerized after a catastrophe event by at least 80% of their initial lengths, whereas in presence of 0.5 μM MAP65-4, MT plus ends did not depolymerize for no more than 50% of their initial lengths. Moreover, after a catastrophe event, single MTs always depolymerized more than 40 to 50% of their initial length, whereas MTs cross-linked by MAP65-4 might depolymerize <20% of their initial length (Figure 5F). As a result, the duration of the shortening phase of MTs bundled by MAP65-4 was decreased compared with that of single MTs, leading to regular growth of MT bundles over time. These measurements were difficult to obtain for MT minus ends, as they were short and it was difficult to identify them precisely when the number of MTs within a bundle was high. Although the duration of MT shortening between catastrophe and rescue events could sometimes be measured and indicated that MTs tended to decrease their depolymerized length after a catastrophe event, the sample size

was insufficient to draw a meaningful comparison with single MTs. Together, these data indicate that MAP65-4 induced a change in dynamic MT behavior; for example, when MTs were organized in bundles by MAP65-4, they exhibited a decrease in their intrinsic dynamic instability, leading to persistent bundle growth. Analysis of the collective dynamic behavior of MTs within a bundle induced by MAP65-4 showed that, for MAP65-4 concentrations of above 0.25 μM , the distance between mean and maxima MT lengths decreased, and this may indicate a global synchronization of MT polymerization within a bundle (see Supplemental Figure 4 online).

In the assays, we observed physical collisions between growing MT bundles (see Supplemental Movie 5 online). When a growing MT bundle end encountered another MT bundle, we observed different responses: the growing MT bundle crossed over the resident MT bundle and continued to grow in 88% of the observed encounters ($n = 173$); underwent catastrophe, which impeded crossing over (7%, $n = 14$); paused (4%, $n = 7$); or coaligned with the resident MT bundle to form a thicker MT bundle (1%, $n = 2$). Coalignment was observed when MTs collided at a shallow angle (<10°; see Supplemental Movie 5 online). The crossing over events were independent of the angle of encounter between two MT bundles.

Dynamics of MAP65-4 MT Binding

We next examined the binding of MAP65-4 on MTs during MT bundle growth (Figure 6). Line scans and kymographs of

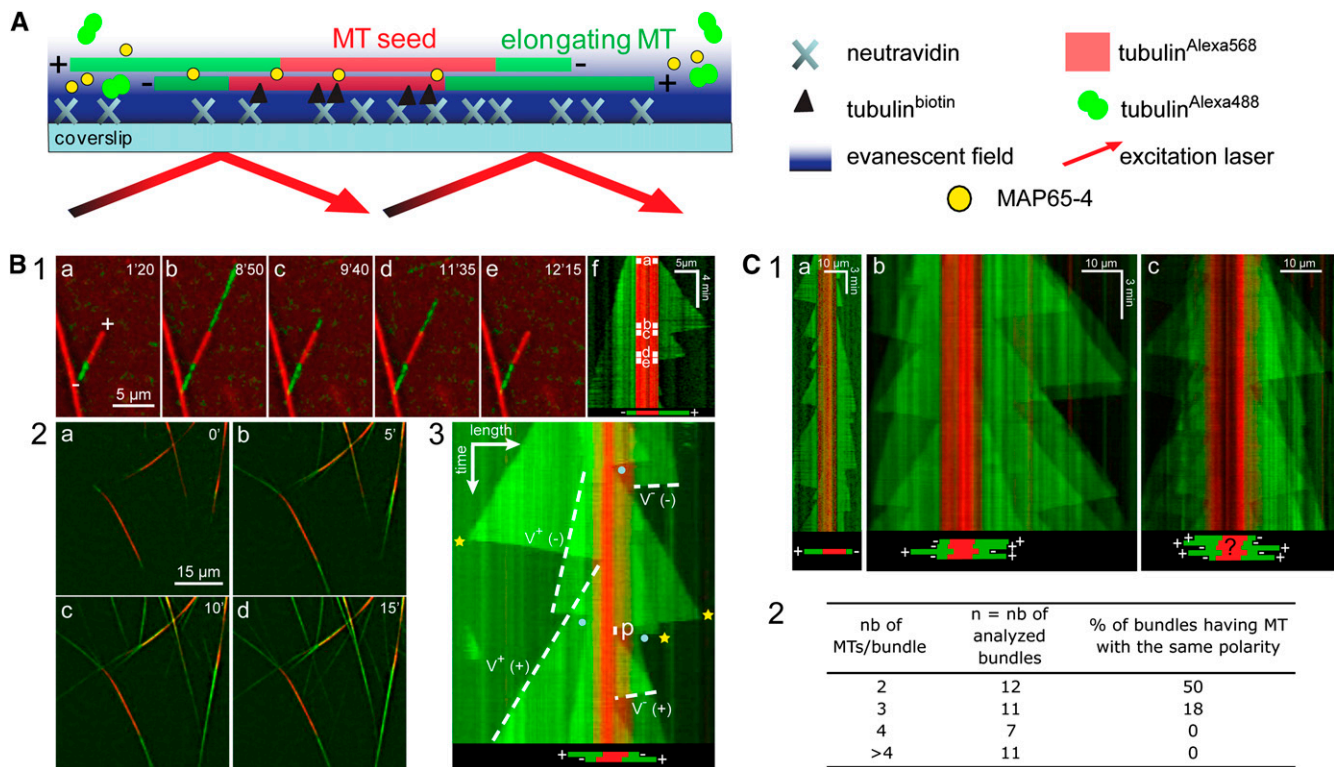


Figure 4. TIRF Microscopy Analysis of MT Polarity within Bundles Induced by MAP65-4.

(A) Diagram of the experimental setup: dynamic elongation of Alexa488-MTs (green) from stabilized GMPCPP Alexa568-MT seed bundles (red) in the presence or the absence of MAP65-4. Seeds (individual MTs or MT bundles referred to as MT seed bundles) were attached to the cover slip via a biotin-tubulin/avidin link. The experiments were performed at 32°C.

(B1) Dual-view image series of an individual MT: the seed (red, 0.3 μ M) was elongated by the addition of Alexa488-labeled tubulin (green, 22 μ M). **(a)** to **(e)** Images extracted from the time-lapse series (see Supplemental Movie 3 online) show the dynamic instability behavior of the elongating MT at both ends. The associated kymograph **(f)** displays the MT elongation/shortening and catastrophe/rescue events.

(B2) Dual-view image series (**[a]** to **[d]**) of MT bundles: seed bundles (0.3 μ M) were grown by adding Alexa488-labeled tubulin (22 μ M) in the presence of AtMAP65-4 (0.15 μ M). After 15 min **(d)**, a dense network of MT bundles was assembled.

(B3) Kymograph example from an elongating MT bundle composed of two MTs. On this kymograph, MT assembly parameters in the presence of MAP65-4 can be determined at both ends (dashed lines): polymerization rate (v^+) and depolymerization rate (v^-), catastrophe/rescue frequencies (yellow stars/blue dots), and duration of pauses (p).

(C1) Analysis of MT polarity within bundles induced by MAP65-4. Kymograph of a single MT **(a)** and MAP65-4-induced MT bundles **(b)** and **(c)**.

(C2) Determination of MT polarity within MT bundles. nb, number. These data demonstrate that the polarity within bundles induced by MAP65-4 is random.

elongating MTs in the presence of GFP-AtMAP65-4 showed that the accumulation of GFP-MAP65-4 along MTs was concomitant with MT polymerization (Figure 6A). In the experimental setup used, the binding of GFP-MAP65-4 to MTs followed polymerization by <2 s, as illustrated by the fluorescent position of Alexa568-labeled tubulin and GFP-MAP65-4 on the kymograph in Figure 6A. In the following experiments, we investigated the turnover rate of MAP65-4 binding to MTs by means of fluorescence recovery after photobleaching (FRAP; Figure 6B). After photobleaching of GFP-MAP65-4, no fluorescence recovery was observed within 30 min in the presence of an excess amount of GFP-MAP65-4. By contrast, GFP-MAP65-4 was incorporated into newly formed MT bundles, indicating that active GFP-MAP65-4 was available throughout the experiment. To confirm that the absence of FRAP was caused by a low MAP65-4

recovery, MT bundles were polymerized for 20 min in the presence of MAP65-4 rather than GFP-MAP65-4 and incubated with GFP-MAP65-4. Once again, we did not observe any exchange of MAP65-4 protein at the MT bundles after 30 min. We therefore conclude that, *in vitro*, the dissociation parameter (k_{off}) of AtMAP65-4 for MTs is very low ($<5.6 \cdot 10^{-4} \text{ s}^{-1}$).

DISCUSSION

The acentrosomal plant mitotic spindle has unique structural properties, such as the absence of the equivalent of two opposing centrosomes at poles and the presence of a connective preprophase band that regulates the spatial and temporal framework for spindle mobility and bipolar spindle establishment.

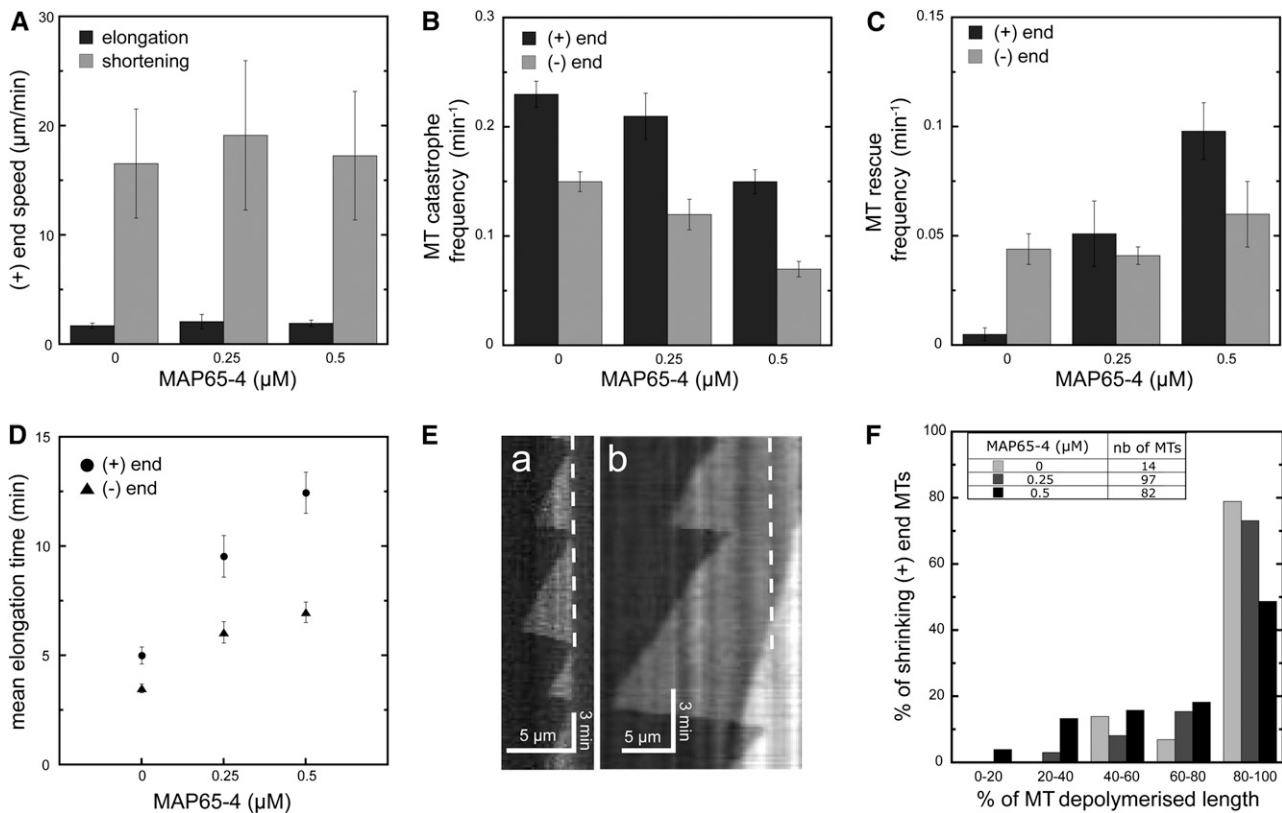


Figure 5. Effects of MAP65-4 on the Dynamic Parameters of MTs within Bundles.

(A) Histogram of the mean elongation and shortening speeds of MT plus ends when bundled by MAP65-4 ($n \geq 20$). Error bars indicate SD.
(B) Catastrophe frequencies measured at the minus and plus ends of MT bundled by different MAP65-4 concentrations. Error bars indicate SE ($n \geq 10$). MAP65-4 decreases the frequency of catastrophe and rescue events at both MT ends.
(C) Rescue frequencies measured at the MT minus and plus ends in the presence of various concentrations of MAP65-4. Error bars represent SE ($n \geq 6$). MAP65-4 has no significant effect on rescue frequencies at the MT minus ends but increases rescue frequencies at the MT plus ends.
(D) Plot of the mean elongation duration of MTs at their plus ends and minus ends when bundled or not by MAP65-4. Error bars indicate SE ($n \geq 38$). MT elongation time increased when MTs were cross-linked by MAP65-4.
(E) Kymographs showing the dynamics of a MT plus end of a single MT **(a)** or of a MT within a bundle **(b)**. Dashed lines delimited MT seed boundary
(F) Histogram illustrating the ratio of the depolymerization rate of the plus ends of single MTs to that of MTs cross-linked by MAP65-4. In the absence of MAP65-4, MT depolymerization occurs mostly until the nonhydrolyzable seed (80% of MT shrinkage events), whereas this occurs in only 50% of MTs cross-linked by MAP65-4.

These properties are most likely a reflection of the characteristics of microtubule-associated proteins (MAPs) and motors. Here, we show that MAP65-4, a MAP that belongs to the MAP65 family, associates with the early mitotic spindle and the kinetochore fibers from prometaphase to anaphase. *In vitro*, MAP65-4 induces MT bundling through the formation of cross-bridges between adjacent MTs. Furthermore, we were able to set up an assay to determine that MAP65-4 modulates the dynamic instability parameters of individual MTs within a MT bundle.

MAP65-4 Cross-Links MTs *In Vitro*

In a previous study, we demonstrated that MAP65-1 and MAP65-5, two other members of the MAP65 family, form a fishbone lattice between antipolar MTs *in vitro* (Gaillard et al., 2008), and more recently Subramanian et al. (2010) showed that

PRC1, the mammalian homolog of MAP65-1, exhibits an identical distribution. MAP65-4 also forms cross-bridges between adjacent MTs, but importantly the cross-bridges (15 nm) are significantly shorter than those generated by MAP65-1/MAP65-5 (30 to 40 nm), despite the proteins having a similar molecular weight and their domains upstream of the MT binding domain being approximately identical in size. The cross-bridges are implanted on the MT lattice at an angle of 90°. Hence, the binding of MAP65-4 to the MT lattice is not stereochemically hindered to interact with polar or antipolar MTs. Indeed, the orientation at which the MTs occurred within MAP65-4 induced bundles was random, indicating that the binding of MAP65-4 to MTs does not favor polar or antipolar MTs (Figure 4C, 2). In live cells, MAP65-4 is preferentially associated with MTs oriented toward the poles, as it localizes at the two polar halves of the forming spindle and with the kinetochore fibers, which point the minus ends toward

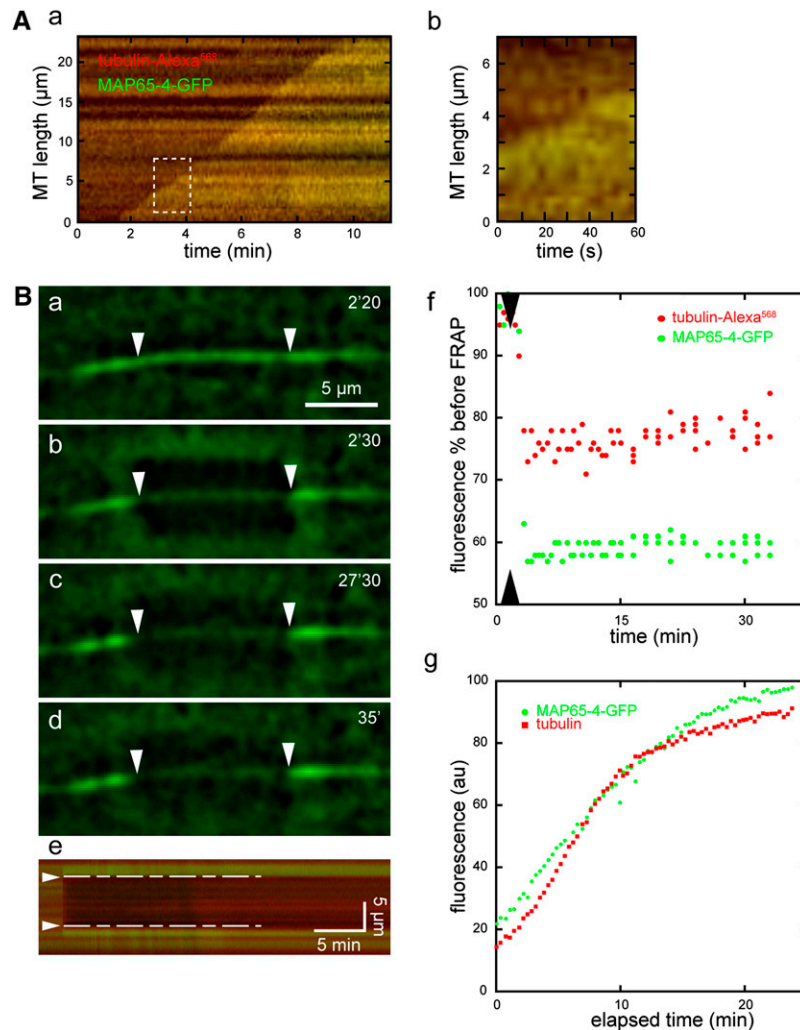


Figure 6. MAP65-4 Binds Rapidly and Durably to Elongating MT Bundles.

(A) Merged kymograph of an elongating MT bundle labeled with Alexa568-tubulin and GFP-AtMAP65-4 **(a)**. An enlargement of the boxed area is shown in **(b)**. MAP65-4 binding is concomitant with MT bundle elongation.

(B) Time-lapse series [**a**] to [**d**] of a photobleached MT bundle and its associated kymograph **(e)**. GFP-MAP65-4 and Alexa568-tubulin fluorescence levels measured by line scans **(f)** of the photobleached area [**e**]; between broken lines). GFP-MAP65-4 fluorescence does not recover after photobleaching **(g)**. Tubulin polymerization and binding of free GFP-MAP65-4 during the assay. These measurements were performed on the entire field of view ($\sim 8.10^{-3}$ mm²) over a 25-min period.

the poles. We therefore speculate that other proteins and/or mechanisms, such as the localization of MT nucleation sites, regulate MT orientation in the early spindle and that their bundling by AtMAP65-4 may occur later.

Effects of MAP65-4 on MTs Dynamics in Vitro

In this study, we used TIRF microscopy to determine the dynamic parameters of individual MTs within MAP5-4-induced MT bundles. We found that MAP65-4 did not alter the intrinsic growth and shrinkage rates of MTs within bundles at both of their ends but that it reduced catastrophe and increased rescue frequencies in a dose-dependant manner. As MAP65-4 predom-

inantly localized along the MTs and not at their ends, and as the rate of (de)polymerization was not altered in the presence of MAP65-4, we speculate that the change in dynamics was the result of stabilization of the GTP/GDP lattice by cross-linking protofilaments of two adjacent MTs and/or two tubulin dimers on a protofilament. The net effect of a reduction in catastrophe events together with an increase in rescue events is that MAP65-4-bundled MTs elongate for a much longer period than single MTs. As a result, MT bundles are more stable than single MTs and progressively elongate, allowing them to potentially extend deep into the cellular space. MAP65-4-stimulated bundling serves as a brake when catastrophe events occur (see schematic drawing in Figure 7) and thus may prolong the half-life of

MTs during mitosis. A recent study on the midzone organization in yeast revealed that Ase1, the homolog of MAP65-1, is required for the reduction in dynamics of the interpolar MTs (Fridman et al., 2009). In plant cells, the dynamics of MTs that colocalized with MAP65-1 and MAP65-5 were analyzed in interphase cells. Previously, it was shown that MAP65-1- and MAP65-5-labeled MTs polymerized at a normal rate but that depolymerization was reduced twofold (Van Damme et al., 2004). Together, these results suggest that MAP65 proteins may regulate MT dynamic behavior by different mechanisms.

FRAP experiments showed that there was no recovery of MAP65-4 bound to MT bundles after 30 min, indicating that its dissociation parameter for MTs is very low. These data suggest that MAP65-4 behaves as tau, a neural MT bundler, which dissociates one molecule every 42 min in vitro (Ross et al., 2004). In vivo, the turnover rate of MAP65-4 might be much faster and could be similar to that of other members of the MAP65 family that have been reported to be in the range of 5 s for MAP65-1

(Chang et al., 2005; Smertenko et al., 2008) and 76 to 111 s for MAP65-3 (Smertenko et al., 2008). We have not attempted to study the MAP65-4 turnover in vivo because this protein does not associate with the interphase cortical arrays. Measuring fluorescence recovery of MAP65-4 within the mitotic spindle is not as reliable as measuring new fluorescent signals, which could correspond to new MT assembly within such a dense structure.

In our in vitro assays, the crossing over events between growing MT bundles were independent of the angle of encounter between two MT bundles. This is different to what has been documented for MT–MT interactions in the plant cortex during interphase, where mobile MTs and MT bundles coalign when the angle of incidence is $<40^\circ$, which allows for the formation of MT bundles in the cell cortex (Wasteneys and Ambrose, 2009). Because MAP65-4 is associated strictly with forming spindles during prophase and then with kinetochore fibers, it might, in contrast with MAP65-1, not participate in the MT–MT interactions that generate MT networks (Wasteneys and Ambrose, 2009). Furthermore, we hypothesize that the steric conformation of MT cross-bridges induced by MAP65-4 may not permit the considerable angles of MT bending required to bundle MTs with preexisting MTs, as described for MT bundles decorated with MAP65-1 within the cells (Wasteneys and Ambrose, 2009).

Spatiotemporal Correlation of MAP65-4 and Its Putative Role in Living Cells

Live-cell imaging of MAP65-4 distribution during the cell cycle of transformed tobacco BY-2 cells showed that its MT binding capacity was restricted to mitosis. At the transcriptional level, MAP65-4 is strongly upregulated at the beginning of mitosis (Van Damme et al., 2004). The presence of a consensus D box in MAP65-4 points to its possible 26S proteasome-dependent degradation during anaphase. Binding of GFP-MAP65-4 to MTs was also spatially regulated, and a selective binding was indeed noticed for centrally localized MTs at the prophase nucleus, while the cortical MTs and the PPB were not labeled by GFP-MAP65-4. During prophase, upon bipolarization of the perinuclear MT array, MAP65-4 started to accumulate at the two sides of the nucleus that corresponded to the future poles of the spindle, then with bundles that invaded the nuclear space at the NEB, and finally with the kinetochore fibers from prometaphase until late anaphase, suggesting that MAP65-4 has a role in the assembly of the acentrosomal bipolar mitotic spindle. The bipolarity of the spindle is initiated by the positioning of spindle poles outside the nuclear envelope where they may assemble (Lloyd and Chan, 2006; Vos et al., 2008). The proteins involved are not yet identified, but one can postulate that motor proteins and other MT binding proteins are instrumental in this process (Nédélec et al., 1997; Lloyd and Chan, 2006). MAP65-4 could be a partner involved in early spindle pole morphogenesis by stabilizing MT bundles focused to the poles. In addition, our observations suggest that MAP65-4 could be involved in the attachment of MTs to the paired kinetochores during prometaphase through the search-and-capture mechanism based on spatially biased MT dynamic instability, as described for centrosomal animal cells (Wollman et al., 2005). In this model, it is proposed that, during NEB, MT plus ends persistently grow

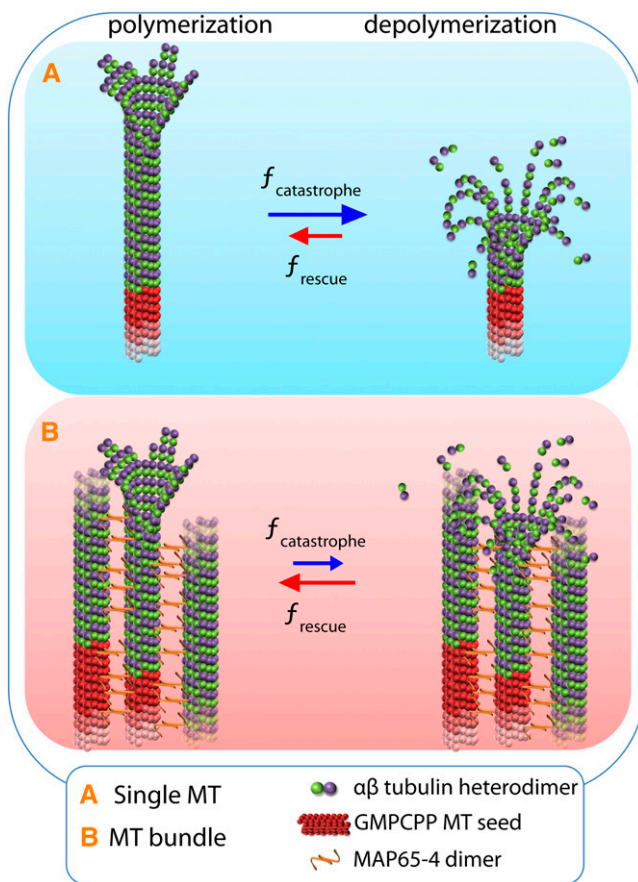


Figure 7. Schematic Summary of How MAP65-4 Facilitates Bundle Growth.

(A) Non cross-linked MTs display dynamic instability behaviors. **(B)** Within bundles, we observed that MAP65-4 acts as a brake and increases the rescue frequencies. This induces an increase in MT elongation duration and thus builds long MT bundles.

toward chromosomes until they capture a kinetochore and that this establishes MT-based connections between chromosomes and spindle poles. To support MT persistent growth, catastrophe frequencies have to be depressed in the region between the poles and the chromosomes. Considering the localization of MAP65-4 and its effects on MT dynamic instability *in vitro*, it is tempting to postulate that MAP65-4 regulates the persistent assembly of MTs searching for kinetochores, presumably with other mechanisms, such as Ran-GTP gradients (Wollman et al., 2005). Besides the search and capture mechanism that underlies the formation of a kinetochore fiber, chromosome-based MT nucleation has been reported to be involved in the formation of acentrosomal and centrosomal spindles (Cleary and Hardham, 1988; Maiato et al., 2004; Chan et al., 2005). Indeed, in animal cells, TPX2 (the targeting protein for Xklp2) has been described to induce MT nucleation at the kinetochore through activation by active Ran GTPase and Aurora kinases (Gruss et al., 2002). Recently, the plant homolog of TPX2 was localized mainly with the two spindle halves from prometaphase to anaphase and may be involved in MT nucleation through its activation by an active Ran GTPase gradient (Vos et al., 2008). The local activation of MT nucleation by TPX2 followed by cross-linking through MAP65-4 activity could participate in the organization and stabilization of kinetochore fibers. Furthermore, MT nucleation via TPX2 activation may occur at the poles of the forming spindle before NEB, as there is a Ran-GTP gradient present there as well as an ortholog of Aurora kinase (Demidov et al., 2005). Thus, by cross-linking MTs and modulating their dynamics, MAP65-4 may stabilize the prospindle and promote bipolarity of the spindle by focusing the MT minus ends at the spindle poles. From these data, an emerging picture appears that strongly suggests that plants have a comparable mechanism to the centrosome-based animal mechanism, which involves spindle bipolarity formation before NEB, although this does not exclude the possibility that kinetochore fibers may nucleate MTs in early prometaphase.

In future work, it will be of great interest to determine the role of AtMAP65-4 in the assembly of plant acentrosomal mitotic spindles by identifying the molecular mechanisms that regulate its activity. The capacity of AtMAP65-4 to modulate MT dynamics within bundles makes it a promising candidate key regulator of spindle formation and organization.

METHODS

Recombinant Protein, Expression, and Purification

Arabidopsis thaliana MAP65-4 domains were purified as tagged proteins with a His tag at the N and C termini, mCherry, or GFP at the N terminus, or a His tag at the C terminus, using vectors as described by Gaillard et al. (2008). Primers used to amplify cDNAs are provided in Supplemental Table 1 online. Three domains were defined: (1) domain 1 (amino acids 1 to 135), domain 2 (amino acids 136 to 320), and domain 3 (amino acids 321 to 648). These domains and AtMAP65-4 deleted of one domain were further referred to as AtMAP65-4(1), AtMAP65-4(2), AtMAP65-4(3), AtMAP65-4(13) (lacks domain 2), and AtMAP65-4(23) (lacks domain 1). All sequences were verified by sequencing. Recombinant AtMAP65-4s proteins were purified on Ni Sepharose columns and stored at -80°C in 10% (v/v) glycerol, 50 mM NaPi, 0.1 M NaCl, and 0.5 mM DTT, pH 7.9, according to Gaillard et al. (2008).

Tubulin Polymerization and MT Binding Assays

Purified bovine tubulin (Vantard et al., 1994) was assembled in G-BRB80 buffer (BRB buffer: 80 mM PIPES, pH 6.8, 1 mM EGTA, and 1 mM MgCl_2 plus 1 mM GTP). Polymerization was monitored at 350 nm at 37°C . For MT binding assays, MTs were assembled from 20 mM unlabeled tubulin in the presence of 20 mM of taxotere (Sigma-Aldrich) in G-BRB80 at 37°C for 30 min and further diluted in MAP buffer (50 mM NaPi, 0.1 M NaCl, and 0.5 mM DTT, pH 7.9) supplemented with 10 mM taxotere. MTs were then incubated with AtMAP65-4s at 20°C for 20 min and sedimented at 100,000g for 10 min at 25°C . Supernatants and pellets were analyzed by SDS-PAGE and immunoblots and probed with anti-AtMAP65-4 antibodies. To analyze the relative efficiencies of the full length and constructs of AtMAP65-4 to bundle MTs, cosedimentation assays were performed at low speed centrifugation (10 min, 4000g, 25°C).

In Vitro Imaging Assays

Fluorescent tubulin (Alexa488-labeled tubulin and Alexa568-labeled tubulin) and biotinylated tubulin were prepared according to Hyman et al. (1991). For conventional fluorescence microscopy, fluorescent taxotere-stabilized MTs assembled from a mixture of fluorescent and unlabeled tubulin were incubated at 20°C in the absence or presence of AtMAP65s and sedimented on cover slips according to Gaillard et al. (2008). Samples were observed using a fluorescence microscope (Zeiss Axio-plan 2 microscope, $\times 63$ magnification, numerical aperture 1.3 objective, Hamamatsu CCD orcal camera, and Metaview image processing). For negative-stain electron microscopy observations, MTs (1 μM) were incubated at 20°C for 20 min with AtMAP65-4 (1 μM). Samples were stained with 2% (w/v) uranyl acetate and observed on a CM12 microscope (FEI Eindhoven) operating at 120 kV. MT dynamic behavior within AtMAP65-4-induced bundles was observed using TIRF microscopy. For the assays, stable MT seeds were obtained by two steps. First, 2.4 μM tubulin (1.9 μM Alexa-labeled tubulin and 0.5 μM biotin tubulin) was assembled in BRB80, 1 mM DTT, and 0.05 μM GMPCPP (Interchim) for 45 min at 37°C . Second, 0.24 μM of assembled MTs were extended by the addition of 2.7 μM tubulin (2.14 μM Alexa-labeled tubulin and 0.56 μM biotin tubulin) for 2 h at 37°C . Seed bundles were obtained by incubating 0.3 μM MT seeds with 0.1 μM AtMAP65-4 for 10 min at room temperature. To keep MT seeds within the excitation field, we used Neutravidin biotin binding protein (Pierce) specific to biotin to adhere MT seeds to the cover glass surface, which had been cleaned before with rounds of ethanol/water washes. MT seeds and MT seed bundles were then elongated by the addition of 22 μM tubulin (17 μM unlabeled tubulin and 5 μM Alexa-labeled tubulin), in the absence or the presence of AtMAP65-4 (range 0.1 to 0.5 μM), 1 mM GTP, an oxygen scavenger cocktail (2 mg/mL glucose, 80 μg /mL catalase, and 0.67 mg/mL glucose oxidase), and 1.5% BSA. Experiments were conducted in a final volume of 5 μL between glass silanized using dichloromethylsilane (Merck) to limit interactions between MTs and the cover glass (Figure 4A). MT dynamics were visualized at 32°C using an objective-based TIRF microscope (Nikon TE2000-E). Excitation was achieved using 491- and a 561-nm lasers to visualize GFP and Alexa488, and mCherry and Alexa568, respectively. Time-lapse microscopy (one frame every 2 s) was performed for 30 min using Metamorph software (version.6.3r7; Universal Imaging), and frames were analyzed using Metamorph; equalize light, basic filter, and flatten background were the filters used to improve the signal/noise ratio. MT bundle elongation and dynamics were analyzed using kymographs generated by Metamorph and analyzed with ImageJ. The statistical significance was determined using Student's *t* test. FRAP experiments were performed during time-lapse acquisition on small ($2 \times 2 \mu\text{m}$) or large ($5 \times 15 \mu\text{m}$) areas for 25 to 100 ms at 100% laser intensity. Fluorescence recovery was observed by measuring fluorescence intensity along line scans on the corresponding kymographs. Tubulin

fluorescence level served as an internal control. FRAP assays were performed on either GFP- or mCherry-AtMAP65-4, with the same results.

Transgenic Cells

Tobacco (*Nicotiana tabacum*) Bright Yellow-2 (BY-2) cells were transformed as described by Geelen and Inzé (2001). Stably transformed BY-2 cells were immobilized in a chambered cover glass system (Lab-Tek) in a thin layer of BY-2 medium containing vitamins and 0.8% of low-melting-point agarose (Invitrogen). Cells were imaged on a Zeiss LSM710 inverted confocal microscope equipped with the ZEN software package using a C-Apochromat $\times 40/1.20$ W Korr M27 water-corrected lens. Excitation was performed with a multi argon laser (458, 488, and 514 nm) using 6% laser line attenuated transmission, a MBS488 dichroic mirror, and a spectral emission window ranging from 500 to 530 nm. Digital gain was set at 1.00, signal averaging was set at 8, and $\times 3$ digital zoom was applied. Time-lapse images were acquired using the multiposition time-lapse acquisition mode of the ZEN software, with a time interval of 4 min and an optical slice thickness of 1.57 airy units (1.34 μm).

Accession Number

Sequence data from this article can be found in the Arabidopsis Genome Initiative or GenBank/EMBL databases under accession number At3g60840.

Supplemental Data

The following materials are available in the online version of this article.

Supplemental Figure 1. Quantification of MAP65-4-GFP Fluorescence Signal within a Transformed Tobacco BY-2 Cell from G2 to Telophase.

Supplemental Figure 2. Colocalization of MAP65-4 with Microtubule Bundles, as Observed with Fluorescence Microscopy.

Supplemental Figure 3. Identification of the MT binding domain of MAP65-4.

Supplemental Figure 4. Collective Behavior of MTs within MAP65-4-Induced MT Bundles.

Supplemental Table 1. Primers Used to Amplify cDNAs Corresponding to Wild-Type and Truncated Forms of MAP65-4.

Supplemental Movie 1. Tobacco BY-2 Cells Expressing MAP65-4-GFP 4, from G2 to Telophase.

Supplemental Movie 2. Tobacco BY-2 Cells Expressing MAP65-4-GFP 4, from G2 to Telophase.

Supplemental Movie 3. Dynamic Instability Behavior of a Single MT Observed Using TIRF Microscopy.

Supplemental Movie 4. Dynamics of MT Bundles Induced by MAP65-4 Observed Using TIRF Microscopy.

Supplemental Movie 5. Encounters of MAP65-4-Induced MT Bundles Observed Using TIRF Microscopy.

Supplemental Movie Legends.

ACKNOWLEDGMENTS

We thank "Physics of the Cytoskeleton and Morphogenesis" team members for helpful discussions and insightful suggestions. This work was supported by Centre National de la Recherche Scientifique and Commissariat à l'Energie Atomique research programs and from French

research ministry support to V.F. D.V.D. is a postdoctoral fellow of the Research Foundation of Flanders.

Received October 19, 2010; revised October 27, 2010; accepted November 10, 2010; published November 30, 2010.

REFERENCES

- Ambrose, J.C., Li, W., Marcus, A., Ma, H., and Cyr, R.** (2005). A minus-end-directed kinesin with plus-end tracking protein activity is involved in spindle morphogenesis. *Mol. Biol. Cell* **16**: 1584–1592.
- Ambrose, J.C., and Cyr, R.** (2007). The kinesin ATK5 functions in early spindle assembly in *Arabidopsis*. *Plant Cell* **19**: 226–236.
- Bratman, S.V., and Chang, F.** (2007). Stabilization of overlapping microtubules by fission yeast CLASP. *Dev. Cell* **13**: 812–827.
- Caillaud, M.C., Lecomte, P., Jammes, F., Quentin, M., Pagnotta, S., Andrio, E., de Almeida Engler, J., Marfaing, N., Gounon, P., Abad, P., and Favery, B.** (2008). MAP65-3 microtubule-associated protein is essential for nematode-induced giant cell ontogenesis in *Arabidopsis*. *Plant Cell* **20**: 423–437.
- Chan, J., Calder, G., Fox, S., and Lloyd, C.** (2005). Localization of the microtubule end binding protein EB1 reveals alternative pathways of spindle development in *Arabidopsis* suspension cells. *Plant Cell* **17**: 1737–1748.
- Chan, J., Jensen, C.G., Jensen, L.C., Bush, M., and Lloyd, C.W.** (1999). The 65-kDa carrot microtubule-associated protein forms regularly arranged filamentous cross-bridges between microtubules. *Proc. Natl. Acad. Sci. USA* **96**: 14931–14936.
- Chan, J., Sambade, A., Calder, G., and Lloyd, C.** (2009). *Arabidopsis* cortical microtubules are initiated along, as well as branching from, existing microtubules. *Plant Cell* **21**: 2298–2306.
- Chang, H.Y., Smertenko, A.P., Igarashi, H., Dixon, D.P., and Hussey, P.J.** (2005). Dynamic interaction of NtMAP65-1a with microtubules in vivo. *J. Cell Sci.* **118**: 3195–3201.
- Chen, R.H.** (2002). BubR1 is essential for kinetochore localization of other spindle checkpoint proteins and its phosphorylation requires Mad1. *J. Cell Biol.* **158**: 487–496.
- Cleary, A.L., and Hardham, A.R.** (1988). Depolymerization of microtubule arrays in root tip cells by oryzalin and their recovery with modified nucleation patterns. *Can. J. Bot.* **66**: 2353–2366.
- Demidov, D., Van Damme, D., Geelen, D., Blattner, F.R., and Houben, A.** (2005). Identification and dynamics of two classes of aurora-like kinases in *Arabidopsis* and other plants. *Plant Cell* **17**: 836–848.
- Dixit, R., and Cyr, R.** (2004). Encounters between dynamic cortical microtubules promote ordering of the cortical array through angle-dependent modifications of microtubule behavior. *Plant Cell* **16**: 3274–3284.
- Ehrhardt, D.W.** (2008). Straighten up and fly right: microtubule dynamics and organization of non-centrosomal arrays in higher plants. *Curr. Opin. Cell Biol.* **20**: 107–116.
- Fridman, V., Gerson-Gurwitz, A., Movshovich, N., Kupiec, M., and Gheber, L.** (2009). Midzone organization restricts interpolar microtubule plus-end dynamics during spindle elongation. *EMBO Rep.* **10**: 387–393.
- Gaillard, J., Neumann, E., Van Damme, D., Stoppin-Mellet, V., Ebel, C., Barbier, E., Geelen, D., and Vantard, M.** (2008). Two microtubule-associated proteins of *Arabidopsis* MAP65s promote antiparallel microtubule bundling. *Mol. Biol. Cell* **19**: 4534–4544.
- Geelen, D.N., and Inzé, D.G.** (2001). A bright future for the bright yellow-2 cell culture. *Plant Physiol.* **127**: 1375–1379.

- Gruss, O.J., Wittmann, M., Yokoyama, H., Pepperkok, R., Kufer, T., Silljé, H., Karsenti, E., Mattaj, I.W., and Vernos, I.** (2002). Chromosome-induced microtubule assembly mediated by TPX2 is required for spindle formation in HeLa cells. *Nat. Cell Biol.* **4**: 871–879.
- Hussey, P.J., Hawkins, T.J., Igarashi, H., Kaloriti, D., and Smertenko, A.** (2002). The plant cytoskeleton: Recent advances in the study of the plant microtubule-associated proteins MAP-65, MAP-190 and the *Xenopus* MAP215-like protein, MOR1. *Plant Mol. Biol.* **50**: 915–924.
- Hyman, A., Drechsel, D., Kellogg, D., Salser, S., Sawin, K., Steffen, P., Wordeman, L., and Mitchison, T.** (1991). Preparation of modified tubulins. *Methods Enzymol.* **196**: 478–485.
- Janson, M.E., Loughlin, R., Loïdice, I., Fu, C., Brunner, D., Nédélec, F.J., and Tran, P.T.** (2007). Crosslinkers and motors organize dynamic microtubules to form stable bipolar arrays in fission yeast. *Cell* **128**: 357–368.
- Li, H., Zeng, X., Liu, Z.Q., Meng, Q.T., Yuan, M., and Mao, T.L.** (2009). *Arabidopsis* microtubule-associated protein AtMAP65-2 acts as a microtubule stabilizer. *Plant Mol. Biol.* **69**: 313–324.
- Lloyd, C., and Chan, J.** (2006). Not so divided: The common basis of plant and animal cell division. *Nat. Rev. Mol. Cell Biol.* **7**: 147–152.
- Maiato, H., Rieder, C.L., and Khodjakov, A.** (2004). Kinetochore-driven formation of kinetochore fibers contributes to spindle assembly during animal mitosis. *J. Cell Biol.* **167**: 831–840.
- Mao, G., Chan, J., Calder, G., Doonan, J.H., and Lloyd, C.W.** (2005). Modulated targeting of GFP-AtMAP65-1 to central spindle microtubules during division. *Plant J.* **43**: 469–478.
- McDonald, K.L., O'Toole, E.T., Mastronarde, D.N., and McIntosh, J.R.** (1992). Kinetochore microtubules in PTK cells. *J. Cell Biol.* **118**: 369–383.
- Molinari, C., Kleman, J.P., Jiang, W., Schoehn, G., Hunter, T., and Margolis, R.L.** (2002). PRC1 is a microtubule binding and bundling protein essential to maintain the mitotic spindle midzone. *J. Cell Biol.* **157**: 1175–1186.
- Müller, S., Smertenko, A., Wagner, V., Heinrich, M., Hussey, P.J., and Hauser, M.T.** (2004). The plant microtubule-associated protein AtMAP65-3/PLE is essential for cytokinetic phragmoplast function. *Curr. Biol.* **14**: 412–417.
- Murata, T., Sonobe, S., Baskin, T.I., Hyodo, S., Hasezawa, S., Nagata, T., Horio, T., and Hasebe, M.** (2005). Microtubule-dependent microtubule nucleation based on recruitment of gamma-tubulin in higher plants. *Nat. Cell Biol.* **7**: 961–968.
- Nédélec, F.J., Surrey, T., Maggs, A.C., and Leibler, S.** (1997). Self-organization of microtubules and motors. *Nature* **389**: 305–308.
- Ross, J.L., Santangelo, C.D., Makrides, V., and Fygenon, D.K.** (2004). Tau induces cooperative Taxol binding to microtubules. *Proc. Natl. Acad. Sci. USA* **101**: 12910–12915.
- Shaw, S.L., Kamyar, R., and Ehrhardt, D.W.** (2003). Sustained microtubule treadmilling in *Arabidopsis* cortical arrays. *Science* **300**: 1715–1718.
- Smertenko, A.P., Chang, H.Y., Wagner, V., Kaloriti, D., Fenyk, S., Sonobe, S., Lloyd, C.W., Hauser, M.T., and Hussey, P.J.** (2004). The *Arabidopsis* microtubule-associated protein AtMAP65-1: Molecular analysis of its microtubule bundling activity. *Plant Cell* **16**: 2035–2047.
- Smertenko, A.P., Kaloriti, D., Chang, H.Y., Fiserova, J., Opatrny, Z., and Hussey, P.J.** (2008). The C-terminal variable region specifies the dynamic properties of *Arabidopsis* microtubule-associated protein MAP65 isoforms. *Plant Cell* **20**: 3346–3358.
- Smirnova, E.A., Reddy, A.S., Bowser, J., and Bajer, A.S.** (1998). Minus end-directed kinesin-like motor protein, Kcbp, localizes to anaphase spindle poles in *Haemaphysalis endosperm*. *Cell Motil. Cytoskeleton* **41**: 271–280.
- Stoppin-Mellet, V., Gaillard, J., and Vantard, M.** (2006). Katanin's severing activity favors bundling of cortical microtubules in plants. *Plant J.* **46**: 1009–1017.
- Subramanian, R., Wilson-Kubalek, E.M., Arthur, C.P., Bick, M.J., Campbell, E.A., Darst, S.A., Milligan, R.A., and Kapoor, T.M.** (2010). Insights into antiparallel microtubule crosslinking by PRC1, a conserved nonmotor microtubule binding protein. *Cell* **142**: 433–443.
- Van Damme, D., Van Poucke, K., Boutant, E., Ritzenthaler, C., Inzé, D., and Geelen, D.** (2004). *In vivo* dynamics and differential microtubule-binding activities of MAP65 proteins. *Plant Physiol.* **136**: 3956–3967.
- Vantard, M., Peter, C., Fellous, A., Schellenbaum, P., and Lambert, A.M.** (1994). Characterization of a 100-kDa heat-stable microtubule-associated protein from higher plants. *Eur. J. Biochem.* **220**: 847–853.
- Vos, J.W., Pieuchot, L., Evrard, J.L., Janski, N., Bergdoll, M., de Ronde, D., Perez, L.H., Sardon, T., Vernos, I., and Schmit, A.C.** (2008). The plant TPX2 protein regulates prospindle assembly before nuclear envelope breakdown. *Plant Cell* **20**: 2783–2797.
- Wasteneys, G.O., and Ambrose, J.C.** (2009). Spatial organization of plant cortical microtubules: Close encounters of the 2D kind. *Trends Cell Biol.* **19**: 62–71.
- Wollman, R., Cytrynbaum, E.N., Jones, J.T., Meyer, T., Scholey, J.M., and Mogilner, A.** (2005). Efficient chromosome capture requires a bias in the 'search-and-capture' process during mitotic spindle assembly. *Curr. Biol.* **15**: 828–832.

**Arabidopsis Kinetochore Fiber-Associated MAP65-4 Cross-Links Microtubules and Promotes
Microtubule Bundle Elongation**

Vincent Fache, Jérémie Gaillard, Daniel Van Damme, Danny Geelen, Emmanuelle Neumann, Virginie
Stoppin-Mellet and Marylin Vantard

PLANT CELL 2010;22;3804-3815; originally published online Nov 30, 2010;

DOI: 10.1105/tpc.110.080606

This information is current as of February 21, 2011

Supplemental Data	http://www.plantcell.org/cgi/content/full/tpc.110.080606/DC1
References	This article cites 41 articles, 21 of which you can access for free at: http://www.plantcell.org/cgi/content/full/22/11/3804#BIBL
Permissions	https://www.copyright.com/ccc/openurl.do?sid=pd_hw1532298X&issn=1532298X&WT.mc_id=pd_hw1532298X
eTOCs	Sign up for eTOCs for <i>THE PLANT CELL</i> at: http://www.plantcell.org/subscriptions/etoc.shtml
CiteTrack Alerts	Sign up for CiteTrack Alerts for <i>Plant Cell</i> at: http://www.plantcell.org/cgi/alerts/ctmain
Subscription Information	Subscription information for <i>The Plant Cell</i> and <i>Plant Physiology</i> is available at: http://www.aspb.org/publications/subscriptions.cfm